PHYSICAL REVIEW B **85**, 045431 (2012)

Transverse focusing of spin-polarized photocurrents

Juerong Li,[1] A. M. Gilbertson,[2] K. L. Litvinenko,[1] L. F. Cohen,[2] and S. K. Clowes[1,*]
[1]*Advanced Technology Institute and SEPNet, University of Surrey, Guildford, United Kingdom GU2 7XH*
[2]*Blackett Laboratory, Imperial College London, Prince Consort Rd., London, United Kindom SW7 2BZ*
(Received 13 October 2011; revised manuscript received 13 December 2011; published 19 January 2012)

We measure transverse magnetically focused photocurrent signals in an InSb/InAlSb quantum well device. Using optical spin orientation by modulated circularly polarized light an electron spin-dependent signal is observed due to the spin-orbit interaction. Simulations of the focusing signal are performed using a classical billiard ball model, which includes both spin precession and a spin-dependent electron energy. The simulated data suggest that a signal dependent on the helicity of the incident light is expected for a Rashba parameter $\alpha > 0.1$ eVÅ and that a splitting of the focusing signal is not expected to be observed in linear polarized photocurrent and purely electrical measurements.

DOI: 10.1103/PhysRevB.85.045431 PACS number(s): 73.23.Ad, 72.25.−b, 71.70.Ej, 85.75.−d

I. INTRODUCTION

Probably the most significant challenge for the practical application of semiconductor spintronics is the ability to produce spin filters that can create and detect the spin of electrons. However, it is also important to consider the control of the spin as it is this that will fulfill the promise of spintronics.[1] InSb is an important material in this respect as the spins are highly sensitive to both electric and magnetic field control.[2] More importantly, in terms of ultimate device speed, it is the spin precession frequency that sets the upper limit. In InSb quantum wells (QWs), the precession frequencies are greater than 1 THz, which has been demonstrated by the measurement of extremely short spin lifetimes of approximately 0.1 ps in these structures.[3] A downside of this is that the transport of spins becomes the limiting factor. Fortunately, advances in the development of the growth of InSb heterostructures,[4] low-temperature electron mobilities of greater than 100 000 $\mathrm{cm^2V^{-1}s^{-1}}$ are now achievable in InAlSb/InSb QWs[5–7] and ballistic transport is evident in devices with greater than μm dimensions, producing spin coherence lengths of 2 μm.[8]

There have been a number of experimental reports of spin detection using ballistic transport[9] and even more have been proposed.[10,11] Spin-dependent transverse focusing is one such route and has been observed in p-GaAs[12] and n-InSb[13,14] QWs. In these experiments, a current is ejected from a quantum point contact (QPC), which then follows a cyclotron orbit due to an applied perpendicular magnetic field. This field can be tuned so that the electron is detected by a second QPC. Due to strong spin-orbit coupling present in these materials, the diameter of this orbit is dependent on the spin orientation and can manifest as a doublet in the focusing signal. In the reported p-GaAs[12] study, the focusing signal was split by approximately 36 mT for a QPC separation (L) of 800 nm. A large in-plane magnetic field was applied to lift the spin degeneracy of the QPCs and produced a spin filtering effect that was detected by the second QPC. A splitting of the focusing signal was also observed in a similar n-InSb QPC structure,[13] although this experiment did not utilize in-plane magnetic fields. The appearance of a triplet in the second-order focusing peak was attributed to certain spin-flip transitions that occur on reflection from the boundary. A recent theoretical review of these studies[15] noted the comparative strengths of energy splitting due to Rashba interaction that would produce such splittings; in a semiclassical description, the splitting of the first focusing peak (ΔB) can be related to the Rashba parameter α by $\Delta B \approx 4m^*\alpha\hbar/eL$, where m^* is the effective mass of the charge carrier, and the related energy splitting is $\Delta E_R = 2\alpha k$. In the p-GaAs[12] study, $\alpha \approx 0.12$ eVÅ, while for the n-InSb structure $\alpha \approx 1$ eVÅ (see Ref. 13) and 2 eVÅ.[14] In the InSb devices, the respective energy splittings of 25 and 68 meV are an order of magnitude greater than would be expected.[16,17] In particular, the 68-meV splitting is approximately one third of the energy gap of InSb and is therefore unrealistic.

Optical orientation of excited carriers allows the possibility to interrogate the separate contributions of the spin populations in a ballistic device. In our study, we report on the transverse focusing of photocurrents in an n-InSb device, which is sensitive to the modulation of optically orientated spins. We also report on a Monte Carlo approach to examine the result of including spin in the standard billiard ball model[18,19] by introducing a spin-dependent energy and spin precession. The paper is organized as follows: Secs. II and III describe the experimental details and results, Sec. IV describes the model followed by a discussion in Sec. V.

II. EXPERIMENTAL

The focusing device was fabricated using a δ-doped InSb/InAlSb QW grown on (001) GaAs substrate by molecular beam epitaxy (MBE). The heterostructure consists of an AlSb (200 nm)/$\mathrm{Al_{0.1}In_{0.9}Sb}$ (3 μm) buffer layer to reduce the lattice mismatch, a 30-nm InSb QW followed by a 50-nm $\mathrm{Al_{0.15}In_{0.85}Sb}$ cap layer, in which a Te δ-doping layer is located 20 nm above the top of the QW.[20] The material has mobility of 156 000 $\mathrm{cm^2V^{-1}s^{-1}}$ and carrier concentration of 4.5×10^{11} $\mathrm{cm^2}$ at 2 K. The device, shown in Fig. 1 was fabricated by electron beam lithography and shallow plasma etching.[20] Contacts 1 and 3 have a width (w) of 500 nm and are separated (center to center) by 1.5 μm (L). Carriers are depleted near the sidewalls due to surface states at the etched edge, resulting in an effective channel width (w_{eff}) of $w_{\mathrm{eff}} \approx 350$ nm.[20] The longitudinal bar has a width of 3μm (W). All measurements were performed in a Cryogenic Ltd cryogen-free 7-T magnet, with optical

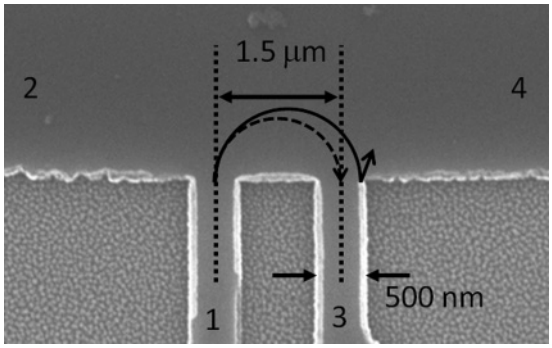

FIG. 1. Scanning electron microscope image of the focusing device, the circular lines represent the path of electrons ejected from contact 1 with differing cyclotron diameters.

access through CaF and ZnSe windows. The focusing signal ($V_3 - V_4$) was measured using a standard ac lock-in technique. For the dark electrical measurements, a 200 nA ac current with a 500 nA dc offset was used to provide a net current between contacts 1 and 2. The photocurrents were produced using a ThorLabs He-Ne 3.4-μm (2–4 mW, 0.37 eV) cw laser mechanically chopped at 1 kHz. The laser energy is sufficient to excite electrons above the subband edge of the InSb QW (≈0.31 eV) but it is far below the energy gap of the InAlSb layers thereby eliminating any parallel contribution from the buffer layer. For these measurements, a 2-V dc voltage was applied across contacts 1 and 2, and a series resistor of 1 MΩ. Quarter-wave modulation of the light was obtained using a ZnSe linear polarizer and photoelastic modulator (PEM) at 37 kHz. The signal response at 1 and 37 kHz was measured simultaneously, which allows both the photoresponse (V_{photo}) and the helicity modulated signal (V_{heli}) to be recorded at the same time. A spherical mirror (focal length of 300 mm) was used to focus the incident light onto the device, where the orientation of the device with respect to this incident beam is shown in Fig. 2. The sample can be rotated so that, using the selection rules for optical interband transitions,[21] spins can be orientated in the x-z plane, where the lead axes are along the y axis. Note that while the sample can be rotated with a known angle θ around the y axis, there is an offset θ_o due to the laser not being incident on the center of the spherical mirror.

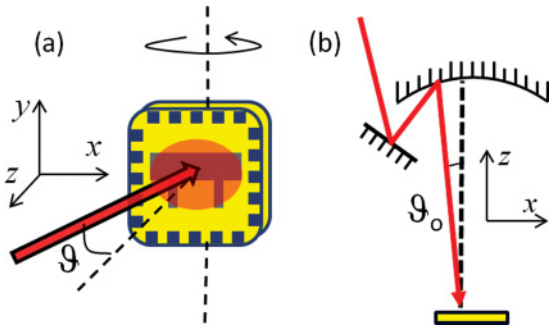

FIG. 2. (Color online) Experimental setup. (a) Chip carrier can be rotated around y axis, where the applied magnetic field direction is along the z axis. θ is the angle between the incident light and a vector normal to the device. (b) $\theta = \theta_o$ when the plane of the QW is perpendicur to the z axis.

III. RESULTS

To compare the properties of the devices with the previously reported experiments,[12–14] we initially took electrical measurements in the "dark," that is, without incident light other than ambient radiation that can enter through the optical windows of the cryostat. These dark measurements were compared with data taken in a radiation shielded nonoptical cryostat (not shown) and were virtually identical demonstrating that the ambient radiation does not create significant changes in carrier density at low temperatures. Dark measurements as a function of temperature are shown in Fig. 3. A characteristic focusing peak is observed at 0.135 T and additional peaks are observed at approximately 0.3 and 0.5 T, which are attributed to the focusing of electrons undergoing one and two sidewall reflections, respectively. Splitting of the first focusing peak is not observed though there is slight shoulder on the higher magnetic field edge. Shubnikov-de Haas oscillations are observed for magnetic fields above 0.5 T, which disappear when the temperature is raised to 20 K consistent with their quantum origin and an energy level broadening of ≈2 meV.[22] All three focusing peaks are observed up to 70 K.

The photoresponse and helicity modulated signals are shown in Figs. 4 and 5, respectively. A strong peak at 0.135 T is observed in both V_{photo} and V_{heli}, which are coincident with the first electron focusing peak in the dark data. There are also many other reproducible features in photoresponse signals, some of which can be attributed to Shubnikov-de Haas oscillations. It should be noted that the peak at 0.185 T in V_{photo} (clearly observed in the 10 K data) cannot be the result of spin splitting of the focusing peak, as a separation of 50 mT would correspond to a total energy splitting of 27 meV, ten times larger than previous theory and experiments. As the temperature is increased, the photoresponse signal decreases, approximately in line with the temperature-dependent decrease of the dark signal. In contrast, the helicity-dependent response has completely vanished by 30 K.

Increasing the in-plane component of the optically orientated spins by rotating the sample has a significant effect on the amplitude of the helicity-dependent signal. In Fig. 6, V_{heli} is shown for θ equal to θ_o, $\theta_o + 15°$, and $\theta_o + 30°$. After each rotation of the sample, the laser is realigned so that the

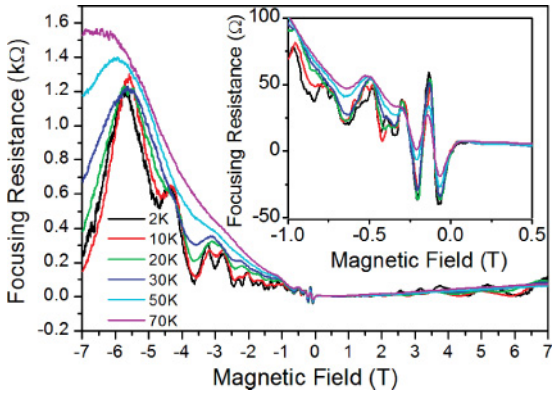

FIG. 3. (Color) Temperature dependence of focusing signal in the dark. Inset: temperature dependence of the three dark focusing peaks in a reduced magnetic field range.

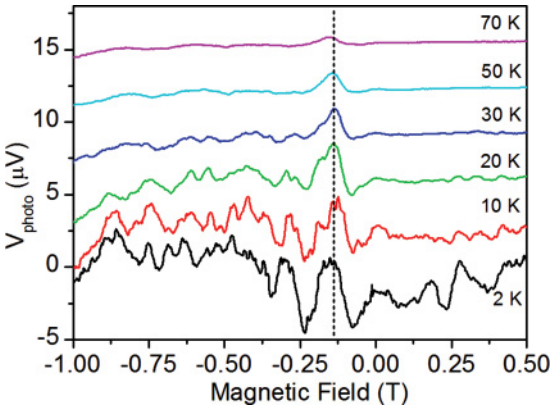

FIG. 4. (Color online) Temperature dependence of photoresponse using linearly polarized light. The plots have been offset by 3 μV for clarity. The dotted line indicates position of focusing signal in the dark at 135 mT. $\theta = \theta_o$.

photoresponse is approximately unchanged. The amplitude of the photoresponse normalized to the 0° value is shown by the squares in the inset of Fig. 6. When the amplitude of the helicity dependence is corrected by dividing by the normalized photoresponse (red line in the inset of Fig. 6), it can be seen that the signal is increased by more than a factor of five for a rotation of 30°. The observed shift of the focusing peak to larger magnetic fields is simply due to the reduced out-of-plane component of the magnetic field ($B\cos\theta$) and therefore larger fields are needed to produce the equivalent cyclotron diameters.

IV. MODEL

Spin-dependent cyclotron motion is often treated in terms of *adiabatic-spin semiclassics*,[23–28] as defined by Zülicke *et al.*[15] In this limit, there are classical trajectories associated with each of the quantized spin states projected along the precession vector, $\mathbf{\Omega}$. This spin projection is kept frozen and as such can be used to describe the splitting in terms of the two possible projections of a $S = 1/2$ electron. Spin precession is not included in this model, where the precession frequency due

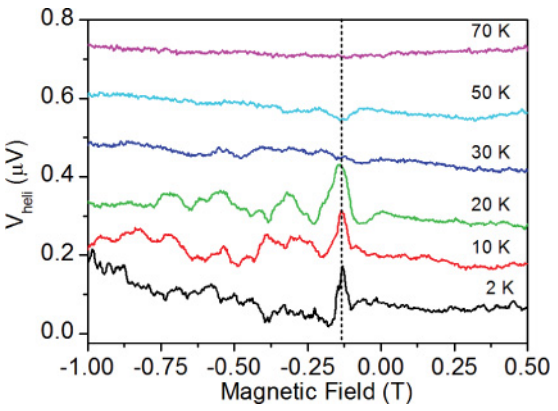

FIG. 5. (Color online) Temperature dependence of helicity signal using modulated circularly polarized light. The plots have been offset by 0.15 μV for clarity. The dotted line indicates position of focusing signal in the dark at 135 mT. $\theta = \theta_o$.

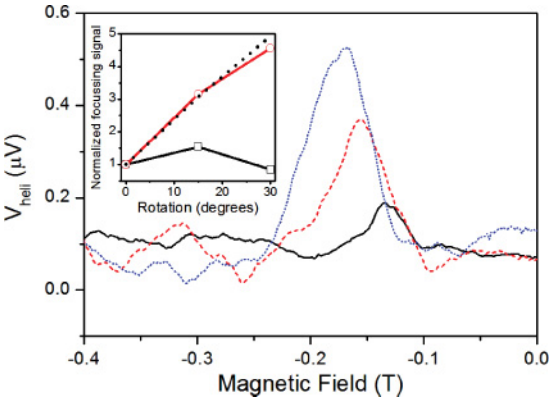

FIG. 6. (Color online) Angular dependence of helicity signal using modulated circularly polarized light, with sample rotated to θ_o (black solid), $\theta_o + 15°$ (red dashed), and $\theta_o + 30°$ (blue dotted) at 10 K. Inset: normalized focusing signals for linear polarized photoresponse (black squares), helicity-dependent photoresponse (red circles), and normalized $\sin(\theta + \theta_o)$ dependence [see Eq. (8)] with $\theta_o = 7°$ (dotted).

to Rashba interaction would be 5.4 THz for $\alpha = 0.1$ eVÅ and $k_f = 1.77 \times 10^8$ m^{-1} compared to the cyclotron frequency of 1.8 THz for InSb at 0.135 T. A fast precession frequency will better allow the spin to follow the evolution of the Rashba precession vector throughout the cyclotron orbit. However, in the event of an abrupt momentum change, for example, scattering from a sidewall, the spin projection along $\mathbf{\Omega}$ will also change. Therefore we should consider the limit described by Zülicke *et al.*[15] of *spin-orbit entwined semiclassics* in which the position, momentum, and spin angular-momentum operators of the electron are intertwined as given by Eq. (3) in Ref. 15. However, there is no reported application of this approach to describe spin focusing or any other spin-dependent ballistic transport effect.

The injection and detection leads in our device are relatively wide compared to typical QPCs employed in electron focusing experiments, and support many transverse modes ($N_{\rm tm} \approx k_F w_{\rm eff}/\pi > 20$). Therefore, in an approach based on the spin-orbit entwined semiclassic limit, we have adopted the Monte Carlo method of simulating ballistic transport using the classical billiard ball model[18,19] with the addition of spin precession and spin-dependent energy terms. In the spin-independent billiard ball model, electrons travel ballistically in circular orbits due to an out-of-plane magnetic field B described by the Lorentz force,

$$\dot{\mathbf{k}} = \frac{eB}{m^*}\begin{pmatrix} k_y \\ -k_x \\ 0 \end{pmatrix}, \qquad (1)$$

where $\mathbf{k}$ is the electron momentum, k_x and k_y are the components of $\mathbf{k}$ in the x-y plane, and m^* is the effective mass. The billiard ball model without including spin works by calculating $\mathbf{k}$, then moving the electron through time interval ΔT and then recalculating $\mathbf{k}$. The magnitude of $\mathbf{k}$ ($=\sqrt{2m^*E_f}/\hbar$) is kept fixed due to energy conservation, where E_f is the Fermi energy with the energy of the subband edge set to zero. Forcing the magnitude of $\mathbf{k}$ to remain constant

is an essential step in the billiard ball model as the finite time interval causes, a propagation of errors that results in the electron spiraling outward rather than forming a cyclotron orbit.

We now include the effects of spin by introducing an additional spin-dependent energy term, so that the total energy is now

$$E_{\text{tot}} = \frac{\hbar^2 k^2}{2m^*} + \frac{1}{2}\sigma\hbar|\mathbf{\Omega}|, \tag{2}$$

where we take this to be conserved and approximately equal to E_f. σ is the projection of spin along $\mathbf{\Omega}$ given by

$$\sigma = \frac{\mathbf{S}\cdot\mathbf{\Omega}}{|\mathbf{S}||\mathbf{\Omega}|}. \tag{3}$$

$\mathbf{\Omega}$ is a function of $\mathbf{k}$ as a consequence of the spin-orbit interaction:

$$\mathbf{\Omega} = \frac{1}{\hbar}\begin{pmatrix} -2\alpha k_y \\ 2\alpha k_x \\ \frac{g\hbar\omega_{c0}}{2} \end{pmatrix}, \tag{4}$$

where g is the effective g factor and $\omega_{c0} = eB/m_0$. Equation (4) includes both Zeeman and Rashba terms but excludes Dresselhaus terms for simplicity (as is appropriate for a highly asymmetric InSb QW[16,17]). The spin $\mathbf{S}$ is evolved using the cross product

$$\dot{\mathbf{S}} = \mathbf{\Omega}\times\mathbf{S} \tag{5}$$

at each time interval ΔT.

The spin term in Eq. (2) can be compared with the quantized description of spin splitting where $\sigma = \pm 1$, so that the spin-dependent energy splitting is $\Delta E = 2\alpha k$ for $B = 0$ and $\Delta E = g\mu_B B$ when $k = 0$. If this spin-dependent term increases, we need to force the momentum to decrease so that energy is conserved, and vice versa. The magnitude of $\mathbf{k}$ is now dependent on the strength and sign of the energy contributions from Zeeman and inversion asymmetry terms. As in the case of the standard billiard ball model, by forcing energy conservation, the previously discussed error propagation is prevented.

Using an iterative process with a suitable time increment ($\Delta T = 1\times 10^{-15}$ s) the path and spin orientation of an electron can be tracked as it travels ballistically through a device. Band parabolicity and single subband occupancy is assumed so that $E_f \approx 2\pi n\hbar^2/2m^*$ and as in the case of Blaikie,[18] electric fields are ignored. Note that in this simple model, spin-dependent terms in the time derivative of the momentum [see Eq. (1)] that appear in the semiclassical model are not included, but due to the small values of α studied here, such terms are expected to be a small perturbation.

We have also adopted the approach of Blaikie *et al.*[18] to introduce diffusive sidewall scattering through the phenomenological parameter p. In this way, an electron on encountering a sidewall can undergo both specular reflection and diffusive scattering, where the probability of specular reflection is defined by p, so that the probability of diffusive scattering is $(1-p)$. A diffusively scattered electron is ejected back into the channel with a cosine distribution $\frac{1}{2}\cos(\phi)$, where ϕ is the angle from the normal to sidewall.

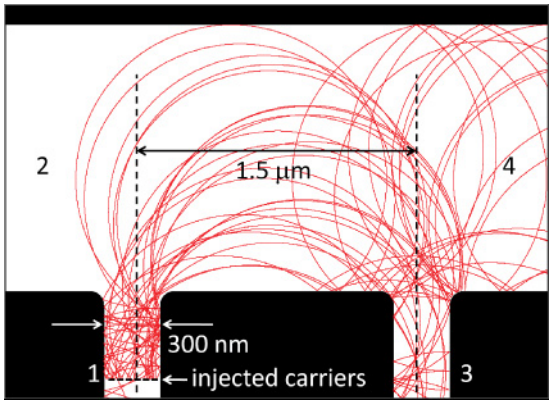

FIG. 7. (Color online) Trajectories of 30 electrons in the simulated focusing device. $n = 5\times 10^{15}$ m^{-2}, $\alpha = 0$, and $B = 0.14$ T.

The geometry of the simulated device is shown in Fig. 7, with $w = 300$ nm and $L = 1.5$ μm. Channels 1 and 3 have a length of 500 nm with corner edges rounded with a radius of 150 nm. Electrons are injected 100 nm from the end of channel 1 (see Fig. 7) with the typical $\frac{1}{2}\cos(\phi)$ due to an assumed square confining potential, where ϕ is the angle between the momentum direction and the axis of the channel. Other variables used in the simulation are $g = 30$,[29] $m^*/m_e = 0.013$, $p = 0.8$,[20] $n = 5\times 10^{15}$ m^{-2}, and $T = 0$ K. The nonlocal resistance of our focusing device ($R_{21,43}$) using Landauer-Büttiker formalism[30] is

$$R_{21,43} = \frac{h}{2e^2}\frac{T_{42}T_{31} - T_{41}T_{32}}{\mathcal{D}}, \tag{6}$$

where T_{ij} is the transmission probability from lead j to lead i and $\mathcal{D}$ is the determinant in Büttiker.[30] If we assume that the ratio of T_{42} and T_{32} is slowly varying with B and that they are comparable in size, then our measured signal will be proportional to $T_{31} - T_{41}$, and so we define

$$T_{\text{foc}} = T_{31} - T_{41}. \tag{7}$$

The simulations for $T_{\text{foc}}(B)$ are shown in Fig. 8 for $\alpha =$ 0.1, 0.2, and 0.5 eVÅ and initial spin orientations of

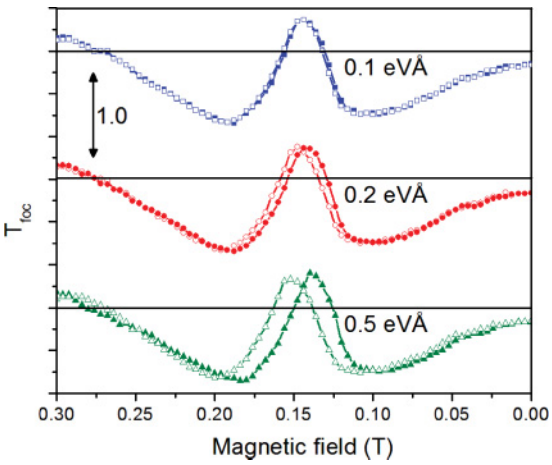

FIG. 8. (Color online) Calculated signal T_{foc} for focusing device shown in Fig. 7 for optical orientations of $S_x = +1$ (solid symbols) and $S_x = -1$ (open symbols) with $\alpha = 0.1$ (blue squares), 0.2 (red circles), and 0.5 eVÅ (green triangles). $N = 8000$ for each data point.

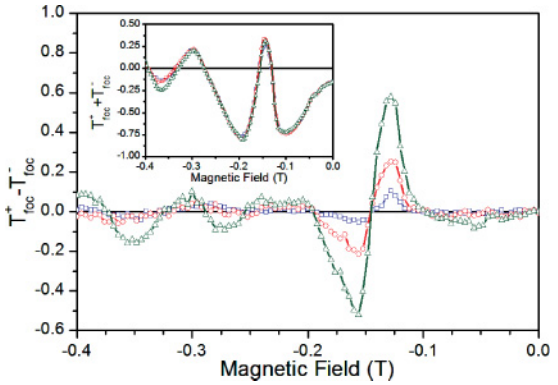

FIG. 9. (Color online) $T_{foc}^{+} - T_{foc}^{-}$ for spins optically orientated $S_x = +1$ and $S_x = -1$. $\alpha = 0.1$ eVÅ (blue squares), 0.2 eVÅ(green circles) and 0.5 eVÅ (red triangles). $N = 8000$ used for $\alpha = 0.3$ and 0.5 eVÅ and increased to $N = 24\,000$ for $\alpha = 0.1$ eVÅ to improve signal to noise. Inset: $T_{foc}^{+} + T_{foc}^{-}$ for simulated data shown in main figure.

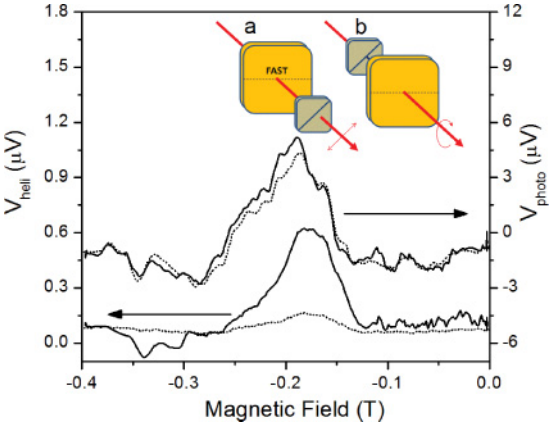

FIG. 10. (Color online) Confirmation that the signal detected at the modulation frequency is due to the degree of circular polarization. V_{photo} and V_{heli} are plotted for linear polarized incident light (solid lines) and circular polarized incident light (dotted lines). The only difference in the two optical arrangements is the position of the linear polarizer, which is placed after the PEM to produce a linear polarized beam (a) and before the PEM to produce a circular polarized beam (b). Both V_{photo} and V_{heli} were recorded simultaneously at $T = 10$ K and $\theta = 30°$.

$S_x = \pm 1$, where each data point is the average of $N = 8000$ trajectories. The smaller value of $\alpha = 0.1$ eVÅ is closer to the values obtained by experiment and theory.[16,17] The simulated curves T_{foc} reproduce well the salient features of the experimental data, namely, the focusing peak and the nonmonotonic background resistance. These focusing peaks have a FWHM of ~33 mT, whereas the splittings of the peaks are only 1, 5, and 13 mT, respectively. A helicity-dependent photocurrent measurement should be sensitive to the difference between T_{foc} for $S_x = \pm 1$, this is shown in Fig. 9. According to our simulation, a large Rashba interaction should result in a large experimentally measured helcity-dependent signal. We note that in the simulated signal, $T_{foc}^{+} + T_{foc}^{-}$ (see Fig. 9), the splitting between the peak (0.13 T) and trough (0.16 T) is approximately the FWHM of the focusing peak rather than the difference in the spin-dependent focusing fields due to the Rashba interaction. In the inset of Fig. 9, we show $T_{foc}^{+} + T_{foc}^{-}$, which reproduces the form of V_{photo} and dark signals, with a clear second focusing peak at ~0.3 T. In the $T_{foc}^{+} - T_{foc}^{-}$ signal for $\alpha = 0.5$ eVÅ, there is an oscillation above 0.2 T, which has a maximum at the second focusing peak position.

V. DISCUSSION

We have observed clear focusing signals (see Figs. 5 and 6) at the modulation frequency of the circular polarization. In this section, we will demonstrate that the origin of this signal is due to spin-dependent transport made visible by the modulated optical orientation of the photoexcited carriers and we will relate our experimental results with the simulated study.

Firstly, it is necessary to confirm that the signals detected at the PEM frequency are due to the helicity modulation and not caused by beam deflections produced by the modulated compression of PEMs birefringent crystal. For this, the focusing signals with linear and circular polarized light were measured without removing the PEM from the optical setup. This was achieved by simply repositioning the linear polarizer to the other side of the PEM (see Fig. 10). As expected, the amplitude of the photoresponse is unaffected by the repositioning of the linear polarizer, while the focusing signal at the PEM modulation frequency is virtually suppressed. This confirms our claim that the helicity-dependent signals are real and not an artifact of the optical setup.

The amplitude of the focusing peak (ΔR) is closely linked to the momentum mean free path ($l_0 = \hbar k_F \mu / e$). Therefore the temperature dependence of ΔR in both V_{dark} and V_{photo} can be attributed to the increased momentum scattering with increasing temperature (see Figs. 3 and 4, respectively). However, the fact that these signals remain visible up to 70 K while the helicity-dependent signal abruptly disappears by 30 K as the temperature is increased (see Fig. 5), strongly supports the assertion of spin-dependent (quantum) origin. The thermal energy at 30 K corresponds to 2.6 meV, which is comparable to a Rashba energy splitting of 3.5 meV for $\alpha = 0.1$ eVÅ and $k_f = 1.77 \times 10^8$ m^{-1}. The Zeeman effect can be neglected as the associated energy splitting at 0.135 T is approximately 0.25 meV and so would not be expected to be visible above 3 K.

The angular dependence of the focusing signals provides the strongest evidence that a spin-orbit interaction is the source of the helicity dependent response. In the following discussion, only the Rashba interaction will be addressed as our theoretical calculations have shown that it should dominate over the Dresselhaus terms in this type of heterostructure.[16] The condition where the strongest spin splitting should occur is when the spins are orientated parallel to $\mathbf{\Omega}$ [see Eqs. (2) and (3)]. In small magnetic fields, $\mathbf{\Omega}$ is dominantly in plane and perpendicular to $\mathbf{k}$ [see Eq. (4)]. As the electrons are ejected from contact 1 with an average momentum in the y direction, the maximum spin splitting for electrons injected into the focusing channel is when $\mathbf{S}$ is along the x direction. Therefore increasing θ will increase the component of the optically orientated spins in x direction and the magnitude of the helicity-dependent focusing peak, as seen in Fig. 6.

In the classical model, the result of $T_{foc}{}^{+} - T_{foc}{}^{-}$ is the case when optical orientation is 100% efficient and the incident light is along the x direction. Note that in this case, σ does not necessarily take values of ± 1 due to the cosine distribution of the initial $\mathbf{k}$ and for increasing magnetic fields, $\mathbf{\Omega}$ is pulled out of the plane. However, in the low field limit ($2\alpha k \gg g\mu_B B$), we can approximate the initial spin population polarization σ_0 induced by optical orientation along the x direction as

$$\sigma_0 \approx \frac{N_+ - N_-}{N} \sin\theta = \frac{1}{2}\sin\theta, \tag{8}$$

where N_+ and N_- are the number of photoexcited electrons with spins orientated in the x-z plane and parallel to the direction of the incident light, N_{tot} is the total number of photo-excited electrons. The factor of $1/2$ comes from the selection rules for InSb. A helicity-dependent signal is observed when rotation $= \sim 0^\circ$ due to the offset θ_o so that even at this orientation with the incident light close to normal incidence there is still a small component of spin orientated in plane. Indeed, the fivefold increase in the helicity dependent peak for a rotation of 30° would be gained if $\theta_o = 7^\circ$, as shown in the inset of Fig. 6. This is consistent with the optical setup.

Whilst the semiclassical spin-dependent billiard ball model contains a number of approximations, in particular, the simplification of the energy relationship in Eq. (2), it is a useful tool to model spin-dependent ballistic transport. We note that the simulated signal $T_{foc}{}^{+} - T_{foc}{}^{-}$ does not reproduce fully the form of the experimental signal $[V_{heli}(B)]$, in that the model predicts a clear peak and trough either side of the focusing field, whereas $V_{heli}(B)$ exhibits a strong peak with only a weak trough. For $\alpha = 0.1$ eV Å, the model does predict a small asymmetry in the form of the focusing signal (blue line in Fig. 9) but not as strong as seen in experiment. A possible cause of this discrepancy is the assumptions made leading to Eq. (7); while we do not expect T_{42}, T_{32}, and $\mathcal{D}$ to have a strong B dependence and thereby introduce additional fine structure to T_{foc}, for the case where $T_{42} \neq T_{32}$, the background signal as a function of B would be altered. Unfortunately, the billiard ball model is ill suited to calculate T_{42}, T_{32}, and $\mathcal{D}$ as the device channel width is large (3 μm) and so localized states and diffusive scattering become significant factors.

VI. CONCLUSIONS

In summary, we have detected the spin orientation of photocurrents using spin-dependent cyclotron motion in a mesoscopic InSb QW device. Furthermore, the semiclassical billiard ball model described in Sec. IV reproduces the experimental results reasonably well. In the experimental data, a splitting of the focusing signal is not observed for the purely electrical, dark measurement for the device shown in Fig. 1 (which is in agreement with the simulation). The reason for this is that the splitting is an order of magnitude smaller than the broadening of the focusing signal. This is due to the relatively large number of transverse modes in contacts 1 and 3, which are very different from the QPCs used in the previous GaAs study.[12] There is also agreement between the experiment and simulation that a helicity-dependent signal should be measurable, and that this signal is associated with the spin orientation of the photoexcited carriers.

ACKNOWLEDGMENTS

We would like to thank B. N. Murdin and A. Kormányos for very useful discussions. J.L. and S.K.C. gratefully acknowledge the support by EPSRC-UK under grant No. EP/E055583-1 and A.M.G. gratefully acknowledges the support by EPSRC-UK under grant No. EP/F065922/1.

*Corresponding author: s.clowes@surrey.ac.uk

[1] S. A. Wolf, D. D. Awschalom, R. A. Buhrman, J. M. Daughton, S. von Molnar, M. L. Roukes, A. Y. Chtchelkanova, and D. M. Treger, Science **294**, 1488 (2001).

[2] K. L. Litvinenko, M. A. Leontiadou, J. R. Li, S. K. Clowes, M. T. Emeny, T. Ashley, C. R. Pidgeon, L. F. Cohen, and B. N. Murdin, Appl. Phys. Lett. **96**, 111107 (2010).

[3] K. L. Litvinenko, B. N. Murdin, J. Allam, C. R. Pidgeon, M. Bird, K. Morris, W. Branford, S. K. Clowes, L. F. Cohen, T. Ashley, and L. Buckle, New J. Phys. **8**, 49 (2006).

[4] T. Ashley, M. T. Emeny, D. G. Hayes, K. P. Hilton, R. Jefferies, J. O. Maclean, S. J. Smith, A. W. H. Tang, D. J. Wallis, and P. J. Webber, 2009 IEEE Int. Electron Devices Meet., 793 (2009).

[5] J. M. S. Orr, A. M. Gilbertson, M. Fearn, O. W. Croad, C. J. Storey, L. Buckle, M. T. Emeny, P. D. Buckle, and T. Ashley, Phys. Rev. B **77**, 165334 (2008).

[6] O. J. Pooley, A. M. Gilbertson, P. D. Buckle, R. S. Hall, L. Buckle, M. T. Emeny, M. Fearn, L. F. Cohen, and T. Ashley, New J. Phys. **12**, 053022 (2010).

[7] S. J. Chung, N. Dai, G. A. Khodaparast, J. L. Hicks, K. J. Goldammer, F. Brown, W. K. Liu, R. E. Doezema, S. Q. Murphy, and M. B. Santos, Physica E **7**, 809 (2000).

[8] R. L. Kallaher and J. J. Heremans, Phys. Rev. B **79**, 075322 (2009).

[9] H. Chen, J. J. Heremans, J. A. Peters, A. O. Govorov, N. Goel, S. J. Chung, and M. B. Santos, Appl. Phys. Lett. **86**, 032113 (2005).

[10] M. Khodas, A. Shekhter, and A. M. Finkel'stein, Phys. Rev. Lett. **92**, 086602 (2004).

[11] A. Shekhter, M. Khodas, and A. M. Finkel'stein, Phys. Rev. B **71**, 125114 (2005).

[12] L. P. Rokhinson, V. Larkina, Y. B. Lyanda-Geller, L. N. Pfeiffer, and K. W. West, Phys. Rev. Lett. **93**, 146601 (2004).

[13] J. J. Heremans, H. Chen, M. B. Santos, N. Goel, W. V. Roy, and G. Borghs, Physics of Semiconductors, Pts A and B **893**, 1287 (2007).

[14] S. Q. Murphy, A. R. Dedigama, D. Deen, N. Goel, J. C. Keay, M. B. Santos, K. Suzuki, S. Miyashita, and Y. Hirayama, Physica E **34**, 647 (2006).

[15] U. Zulicke, J. Bolte, and R. Winkler, New J. Phys. **9**, 355 (2007).

[16] M. A. Leontiadou, K. L. Litvinenko, A. M. Gilbertson, C. R. Pidgeon, W. R. Branford, L. F. Cohen, M. Fearn, T. Ashley, M. T. Emeny, B. N. Murdin, and S. K. Clowes, J. Phys. Condens. Matter **23**, 035801 (2011), this paper calculated the strength of the Rashba and Dresselhaus terms for a 20 nm modulation doped InSb QW at 77 K to be 0.05 and 0.015 eVÅ, respectively.

[17] A. M. Gilbertson, M. Fearn, J. H. Jefferson, B. N. Murdin, P. D. Buckle, and L. F. Cohen, Phys. Rev. B **77**, 165335 (2008).
[18] R. J. Blaikie, D. R. S. Cumming, J. R. A. Cleaver, H. Ahmed, and K. Nakazato, J. Appl. Phys. **78**, 330 (1995).
[19] C. W. J. Beenakker and H. van Houten, Phys. Rev. Lett. **63**, 1857 (1989).
[20] A. M. Gilbertson, D. Benstock, M. Fearn, A. Kormanyos, S. Ladak, M. T. Emeny, C. J. Lambert, T. Ashley, S. A. Solin, and L. F. Cohen, Appl. Phys. Lett. **98**, 062106 (2011).
[21] S. Pfalz, R. Winkler, T. Nowitzki, D. Reuter, A. D. Wieck, D. Hagele, and M. Oestreich, Phys. Rev. B **71**, 165305 (2005).
[22] A. M. Gilbertson, W. R. Branford, M. Fearn, L. Buckle, P. D. Buckle, T. Ashley, and L. F. Cohen, Phys. Rev. B **79**, 235333 (2009).
[23] R. G. Littlejohn and W. G. Flynn, Phys. Rev. A **44**, 5239 (1991).
[24] R. G. Littlejohn and W. G. Flynn, Phys. Rev. A **45**, 7697 (1992).
[25] J. Bolte and S. Keppeler, Ann. Phys. **274**, 125 (1999).
[26] C. Amann and M. Brack, J. Phys. A: Math. Gen. **35**, 6009 (2002).
[27] M. Pletyukhov and O. Zaitse, J. Phys. A: Math. Gen. **36**, 5181 (2003).
[28] A. Kormanyos, Phys. Rev. B **82**, 155316 (2010).
[29] K. L. Litvinenko, L. Nikzad, C. R. Pidgeon, J. Allam, L. F. Cohen, T. Ashley, M. Emeny, W. Zawadzki, and B. N. Murdin, Phys. Rev. B **77**, 033204 (2008).
[30] M. Buttiker, Phys. Rev. Lett. **57**, 1761 (1986).